ROTORCRAFT SIMULATION FIDELITY FOR LOW SPEED MANOEUVRING USING 'ADDITIVE' SYSTEM IDENTIFICATION

Dheeraj Agarwal,
Linghai Lu[1]

Liverpool John Moores University
Liverpool, U.K.

Gareth D Padfield
Neil Cameron
Mark D White

The University of Liverpool,
Liverpool, U.K.

Abstract

High fidelity rotorcraft flight simulation relies on the availability of a quality flight model that further demands a good level of understanding of the complex nonlinearities arising from aerodynamic couplings and interferences. This paper explores rotorcraft flight dynamics in the low-speed regime where such nonlinearities abound and presents a new Additive System IDentification (ASID) approach in the time-domain to aid investigations of these complexities. The ASID approach identifies flight model parameters sequentially based on their contribution to the local dynamic response of the system, in contrast with the averaged values of conventional System IDentification (SID) approaches over a whole manoeuvre. The identified 4 degree-of-freedom model shows good predictability using flight test data from the National Research Council's Bell 412 at hover and how the identified parameters can be used to improve the fidelity of Liverpool's baseline FLIGHTLAB model of the Bell 412. The approach is also used to study nonlinearities attributed to Manoeuvre Wake Distortion (MWD). A cubic rate term is proposed to model the MWD nonlinearities and first results show good correlation for this nonlinear model structure, demonstrated by its capability to capture the nonlinear response and variations of the stability and control derivatives with response magnitude.

NOTATION

g	Acceleration due to gravity [ft/s^2]
p, q, r	Angular velocity components of helicopter about fuselage x, y, z axes [deg/s, rad/s]
$\dot{p}, \dot{q}$	Pitch and roll acceleration [deg/s^2, rad/s^2]
u, v, w	Translational velocity components of the helicopter about fuselage x, y, z axes [ft/s]
$\dot{u}, \dot{v}$	Rates of change of translational velocities [ft/s^2]
x_i	i^{th} state/control variable
I_{xz}	Product of inertia about the helicopter x and z axes [slug-ft^2]
k_p, k_q	Gain [n/d]
L, M, N	External aerodynamic moments about the x-, y- and z-axes (ft lbf)
L_v, M_q etc	Moment derivatives normalised by moments of inertia [rad/s-ft, 1/s etc]
L_{Xa}, etc	Control derivatives normalised by moments of inertia [rad/(s^2-inch) etc]
N	Number of identified derivatives
T_j	Local time-period for identifying x_i^{th} derivative at the jth step [s]
X_a, X_b	Pilot lateral and longitudinal stick input [inch]
X_v, X_p,etc	X force derivatives normalised by aircraft mass [1/s, ft/(s rad) etc.]
Y_v, Y_p,etc	Y force derivatives normalised by aircraft mass [1/s, ft/(s rad) etc.]
Z_v, Z_p,etc	Z force derivatives normalised by aircraft mass [1/s, ft/(s rad) etc.]
β_{1s}	Lateral cyclic flapping angle [deg]
τ_f	Rotor flap time constant [s]
$\tau_{Xa\dot{p}}$ etc	Effective time delay between stick input and related acceleration [s]
δ_{Xa}, δ_{Xb}	Lateral and longitudinal cyclic control displacements [inches]
θ_{1c}	Lateral cyclic pitch angle [deg]
θ, ϕ	Euler angles [deg, rad]
$\dot{}$	Derivative with respect to time

1. INTRODUCTION

The ability to replicate 'real-world' flight behaviour in a virtual environment is key for high-fidelity flight simulation, enabling pilots to train to operate aircraft and designers to evaluate and optimise concepts. Rotorcraft flight training devices are certified using the procedures in documents from regulatory authorities such as EASA's CS-FSTD(H) [1] and the FAA's CFR 14 Part 60 [2]. These detail the fidelity requirements to meet "fit for purpose" approval, defining the acceptable

[1] Corresponding author, Lu, Linghai L.Lu@ljmu.ac.uk, Senior Lecturer in System Modelling Engineering (UAV)

Presented at 45th European Rotorcraft Forum, Warsaw, Poland, 17-20 September, 2019

differences between flight simulation (FS) and flight-test (FT), typically ±10% for flight model tolerances. To reach the highest (CS-FSTD(H) level D) fidelity, it is permitted to achieve this match by modifying, or tuning, the parameters of the FS model using either physics-based or non-physics-based procedures.

System IDentification (SID) has been applied as an effective approach for informing these tuning processes [3,4]. SID can be described as a rational and systematic approach for supporting the development and validation of aircraft flight dynamic models using FT data. The SID approach has been extensively used for fixed-wing aircraft [5-7] and rotorcraft [4,8-17] for performance and handling qualities evaluation, control law development, aircraft dynamic loads analysis, and the creation of models for use in piloted simulation environments.

SID can be performed in either the frequency domain [10] or time domain [7]. In the former, identification of a model is usually performed using control frequency sweeps, while the latter uses multi-step control excitation signals such as doublets, 2311s etc. For rotorcraft, it is common to use SID to identify parameters in the fully coupled 6 degree-of-freedom (DoF) linear models (i.e. the stability and control derivatives), as these can be used to describe the stability and small amplitude response for the rigid-body dynamics. One important key to the success of SID is the availability of good-quality FT data, but there are challenges in obtaining suitable data for rotorcraft in hover and low-speed flight regimes, as the test data often exhibit low signal-to-(process)-noise ratios and can possess strong nonlinearities resulting from the complex aeromechanics. Furthermore, the bare airframe helicopter configuration in hover requires corrective inputs from a pilot during FT to prevent large state deviations from the trim condition, particularly when trying to obtain sufficiently long responses to capture the low-frequency information needed for identification of translational velocity derivatives. This leads to input/output correlation problems and the characteristics of bare airframe rotorcraft responses in hover and low speed pose challenges in the use of traditional SID approaches.

In previous work at the University of Liverpool (UoL) [4], a frequency domain SID renovation technique was developed to improve the fidelity of a FLIGHTLAB [18] Bell 412 (F-B412) simulation model, and the identified model was compared with FT data over a range of forward flight conditions. The FT data are from trials conducted on the National Research Council's (NRC) Advanced Systems Research Aircraft (ASRA) Bell 412 helicopter. A group of candidate SID derivatives (having a high impact on the fidelity 'cost-function' metrics) were used to improve the off-axis responses of the model. Although efficient for improving the fidelity of the simulation model, this tuning approach does not necessarily reveal the physics responsible for modelling discrepancies. This work continues in the Rotorcraft Simulation Fidelity (RSF) project [17,19] involving the UoL, Liverpool John Moores University and the NRC, aimed at developing a physics-based toolset for flight-model fidelity enhancement.

As part of the RSF project, a new approach to SID in the time-domain is being developed and is presented in this paper. We refer to this method as Additive System IDentification (ASID), with the model parameters identified sequentially, or additively, based on their contribution to the local dynamic response of the system, i.e. over a defined time range. One or more candidate parameters in a proposed model structure are identified using the primary response characteristics of the rotorcraft; others are then identified in a sequential manner. The approach is detailed in this paper which includes application to the creation of extended linear and non-linear models to capture and describe the response to multi-step control inputs from a nominal hover condition.

2. EXPLORATION OF NONLINEARITIES

2.1. Modelling Challenges in Low-Speed Manoeuvres

Figure 1 is a sketch of a helicopter accelerating into forward flight from the hover. The rotor wake visualisation is extracted from a vorticity particle method (VPM) computation [20]. The wake dynamics are extremely complex and the effects on the fuselage and empennage loads are equally complex. Separating cause and effect here is difficult.

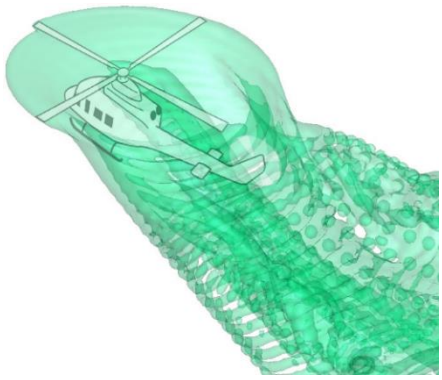

Figure 1 Sketch of rotor wake bathing the fuselage and empennage in low-speed flight

In hover, the horizontal tail is already immersed in the wake and as forward speed increases, the

effects are unsteady but also hysteretic, i.e. the velocity field at the tail is dependent on the rotor loading at previous times. The consequent motion of the helicopter is also likely to be related to the rotor and empennage loads in a nonlinear manner. Modelling the unsteady and nonlinear effects in a way that enables the stability and response to small perturbations to be derived is a challenge that this paper addresses.

2.2. Nonlinearities Associated with Translational Velocities

2.2.1. Nonlinear Responses

In this section, we consider the classical 6DoF linear model and compare the responses with the corresponding nonlinear model for different amplitude control inputs. The baseline model is the UoL developed FLIGHTLAB F-B412 [17]. The model features various options for wake modelling. Initially we consider the version with only the finite-state dynamic-inflow operational.

Figure 2 compares the responses in hover for three different magnitudes of lateral cyclic 2311 input; 0.25, 0.5, 0.75in. To highlight the comparison, all responses are scaled to the lowest input size; the responses for the 0.75in case are therefore divided by three. For a linear model, the scaled responses for the three different input sizes would give the same magnitudes, a situation which will not hold true for the nonlinear model. In particular, the surge and sway velocities reflect nonlinear (Nlr) behaviour as the amplitude of the input increases. The body attitudes θ shows strong nonlinear variations after around 5 seconds.

The initial body rates of the nonlinear model match well with the linear response and start to deviate after about 3sec for the yaw rate and about 5sec for the pitch rate. The attitude and translational velocity perturbations are closely linked of course.

During the final second of the manoeuvre, the scaled roll and pitch rates are very different from the linear responses. This will have a large impact on the relative contribution of terms such as $L_p p$ and $L_q q$, for example, to the overall roll moments. Values of these derivatives identified for small amplitude motion will likely distort the relative contributions from other states as the manoeuvre progresses.

In Figure 3, the responses are compared for different amplitudes of longitudinal cyclic 2311 inputs. For the initial 2 seconds, the rate responses for the nonlinear model match closely with the linearised model for different input sizes. The responses in yaw and heave start to deviate from the linear response early, at around 2.5sec, and the difference increases as the size of the input is increased, revealing nonlinearities in the response with the increasing input size. This is generally due to more excitation energy content as the input amplitude becomes larger [21]. After about 5sec the sway velocity deviates from the linear response, with the minimum just after 6sec indicating a relative contribution of effects like $L_v v$ in the linear model.

The variation of the stability and control derivatives with trim flight speed can provide some clues as to the changing contributions to the different forces and moments as both surge and sway velocities increase. In the following section the derivatives are computed using the conventional backward-forward differencing technique with very small perturbation sizes (2% of trim value).

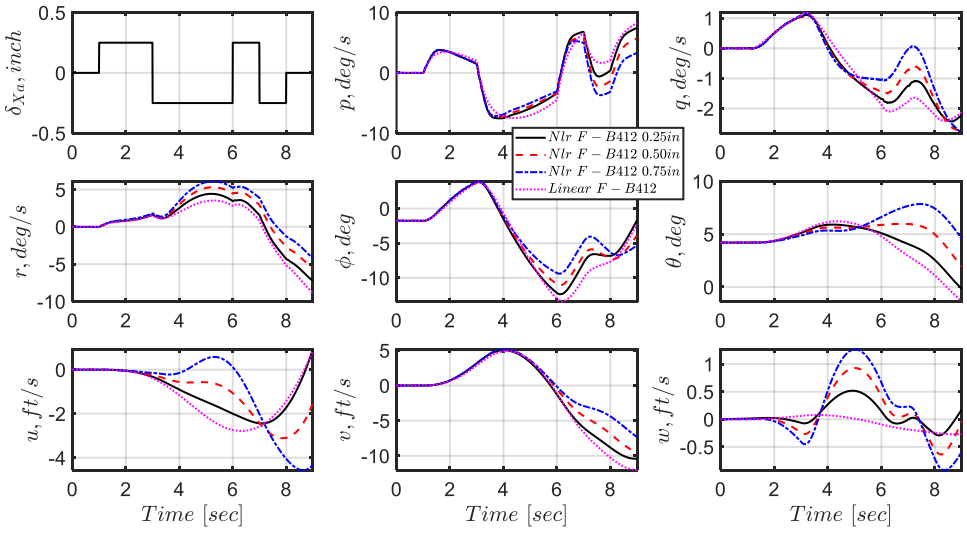

Figure 2 Comparison of the linear and Nlr F-B412 responses for different amplitudes of lateral cyclic 2311 input scaled to the lowest size input.

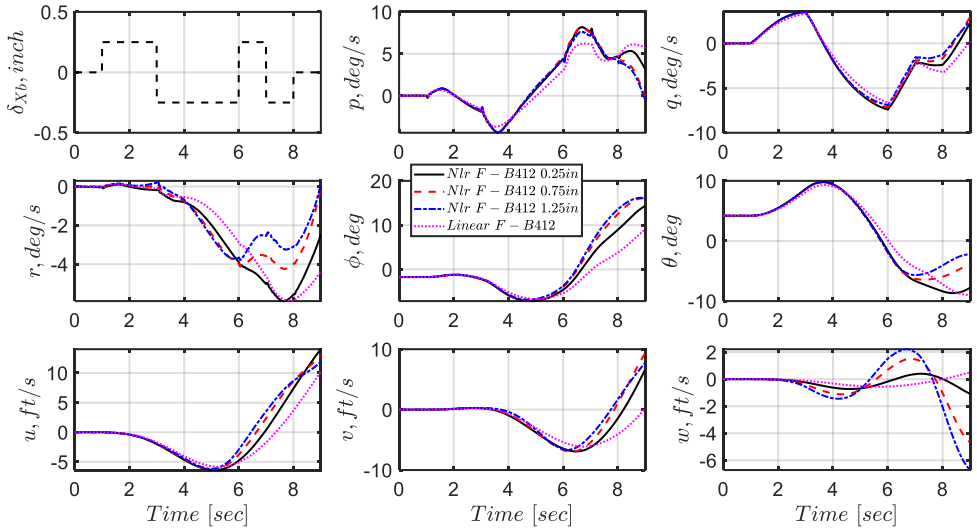

Figure 3 Comparison of the linear and Nlr F-B412 responses for different amplitudes of longitudinal cyclic input scaled to the lowest size input.

2.2.2. Stability Derivative Estimates

As discussed previously, high fidelity modelling is considered a challenging task in the low-speed regime due to the strong rotor-wake effects, so special emphasis is given to describing the variation in the main rotor forces and moments as the trim velocity is increased up to 30kts. There are 36 stability and 24 control derivatives in the 6DoF linear model. The variation of these as a function of flight speed is shown in the Appendix.

Figure 4 illustrates this variation for a selection of derivatives, comparing results for the baseline model with results including manoeuvre wake distortion (MWD) effects [17]. The speed derivative M_u plays a major role in the longitudinal stability and dynamic response of the helicopter. The values of this derivative show that the rotorcraft exhibits static speed stability in hover ($+M_u$) and low-speed flight.

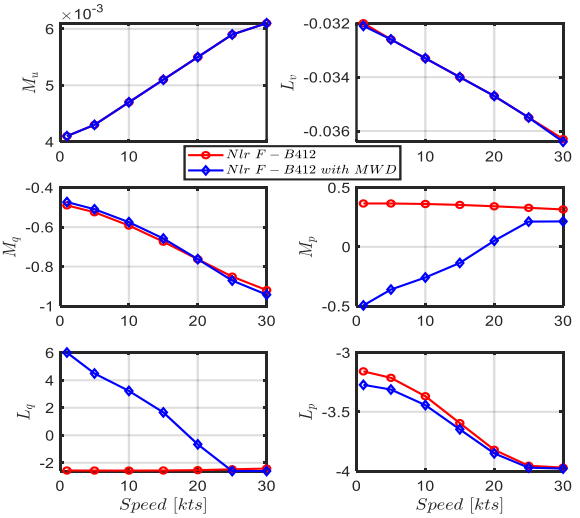

Figure 4. Stability derivatives of the F-B412; comparison with and without MWD effects

The magnitude of the sideslip derivative L_v determines the lateral static stability of the rotorcraft: negative values of L_v are stabilising. Analysing the effect of trim velocity, it is seen that the cross-damping derivatives L_q, M_p are constant without the MWD effect but show almost linear reductions with speed when MWD is added. Close to hover, MWD reverses these cross couplings, a situation already discussed in detail in [17]. The roll and pitch damping derivatives L_p and M_q are predicted to increase by approximately 20% and 80% respectively from 1 to 30 knots.

2.3. Nonlinear Issues in Frequency Domain

One of the concerns of SID processes is the limited range of flight condition over which identified linear models are accurate. SID in the frequency domain produces a quasi-linear describing function, which best models the nonlinear responses, representing the input-to-output relationship under examination. The coherence in the frequency domain analysis indicates whether the system has been satisfactorily excited in the frequency range of interest, and also if the system being modelled can be characterised as linear in this frequency range. When the nonlinearities increase in a model structure, the coherence can be degraded, as illustrated in Figure 5 using Eq. (1),

$$\dot{p} = L_{X_a} X_a + L_p p(1 + k_p p^2) \qquad (1)$$

in which different k_p values associated with the nonlinear term p^3 term are used to model the different strength of nonlinearity, with L_p = -2.95 and L_{xa} = 0.897. The cubic roll rate term reflects the first asymmetric nonlinearity in the Taylor expansion of the aerodynamic moment about the trim condition. Eq. (1) is used to compute the p

response to a 2311 lateral cyclic input in time and frequency domains as shown in Figure 5(a) and (b) respectively, where the effects of the non-linearity are evident, e.g. the increased effective damping at the rate peaks. In the frequency domain, with the increasing value of k_p, the coherence begins to degrade after 5 rad/s, although does not reduce below 0.8 until about 10rad/sec. This sustained level of good coherence can give the analyst the wrong impression about the veracity of the linear relationship.

As discussed in the previous section, rotorcraft in hover and low-speed possess strong nonlinearities resulting from the complex aero-mechanical effects. Furthermore, while obtaining the flight test data for the SID analysis using frequency sweep techniques, these nonlinearities contribute to the drift of the helicopter from the trim condition, requiring corrective control inputs to keep the aircraft close to the trim. However, these secondary inputs should not be strongly correlated with the primary on-axis input, as this will affect the identification accuracy or the coherence. The time domain method described in this paper circumvents this problem by allowing for a time-varying, nonlinear model structure.

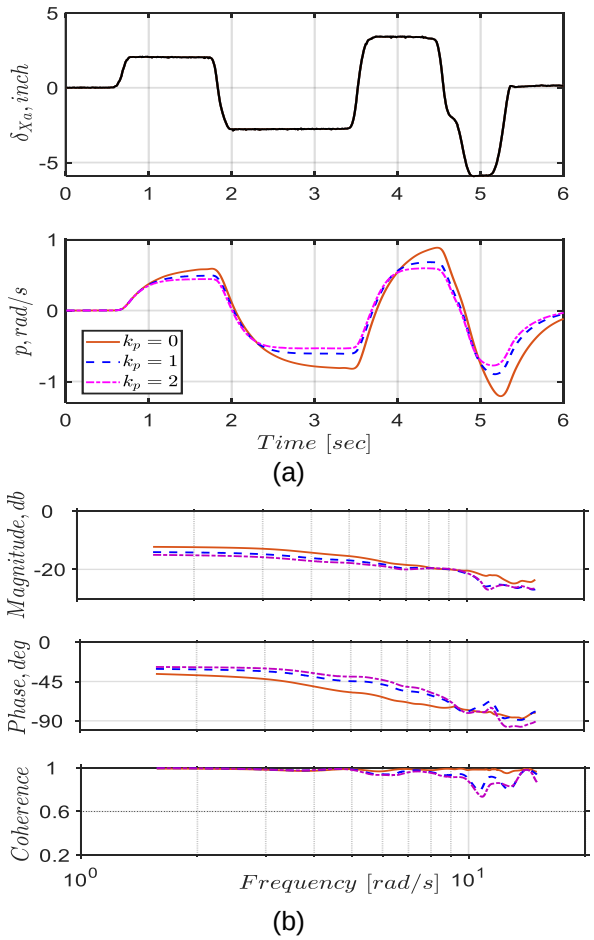

Figure 5 Illustration of the influence of nonlinearity in (a) time domain, (b) frequency domain

3. ASID DEVELOPMENT AND RESULTS

3.1. Response comparison: Nlr F-B412 vs Flight Test

To illustrate the ASID methodology, responses from the Nlr F-B412 will be compared with those from FT. A preliminary comparison is shown in Figure 6. Here, the Nlr F-B412 includes the 3-state Peter-He inflow [22] but does not include aerodynamic interference on the fuselage and empennage due to rotor wake. Results are compared with and without the MWD effects. The FLIGHTLAB MWD model, including a description of its structure and underlying assumptions is presented in [23]. The principal contribution from the MWD inflow model is to reverse the off-axis response as shown in Figure 6; the rotor blades descend into or rise out of the rotor wake during pitch and roll manoeuvres, leading to radial incidence changes that counter the linear aerodynamic effects.

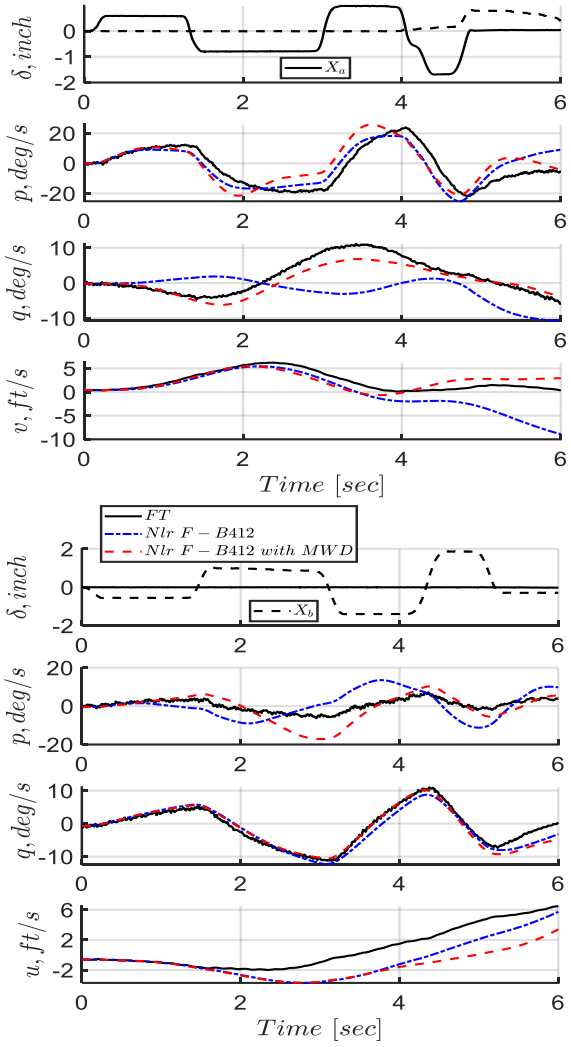

Figure 6 Comparison of dynamics between Nlr F-B412 (with and w/o MWD) and FT (upper, lateral and lower, longitudinal)

The Nlr F-B412 model generally shows reasonably good on-axis response correlation with FT, for both cyclic inputs. MWD improves the off-axis responses. The sway velocity has a good initial match and MWD preserves this through the manoeuvre. The surge velocity departs from the FT after 2sec, but in both manoeuvres the translational velocity perturbations remain small. These rough comparisons can provide some insight into the fidelity of the model and inform the ASID analysis in this Section in two areas: the variation of the relative significance of each response as the manoeuvre progresses, and when and how the translational velocities play their roles and interact with angular motion responses.

3.2. ASID Methodology

In the ASID approach, the model parameters are identified sequentially in an additive manner, based on their contribution to the local dynamic response of the system, i.e. over a defined time range [17]. The detailed ASID approach is outlined in this section with the Nlr F-B412 response for roll dynamics, using an equation-error (EE) process in the time domain, to illustrate its effectiveness, and to develop guidelines for the process.

The linearised roll equation can be written in the usual form,

$$\begin{aligned}\dot{p} = L_{X_a} X_a(t-\tau_{x_a\dot{p}}) + L_u u + L_w w \ldots \\ + L_q q + L_v v + L_p p + L_r r\end{aligned} \quad (2)$$

where *u*, *v*, and *w* are the perturbation translational velocities from trim in the body frame, *p*, *q*, and *r* are the perturbation angular velocities in the body frame; X_a is lateral stick input and *L* represents the normalised roll moment (i.e. roll acceleration); $\tau_{x_a\dot{p}}$ is the (effective) time delay between X_a and roll acceleration. The first step of the ASID approach is to estimate the time delay that is a well-known issue for SID approaches in both the time-domain and frequency-domain.

The effective time delay ($\tau_{x_a\dot{p}}$) is included in Eq. (2) to account for unmodelled higher-order dynamics such as the rotor flap and inflow response, and the control system/actuator delays/lags [10,24]. Techniques for estimating $\tau_{x_a\dot{p}}$ are available, such as the linear backward extrapolation in time to the trim amplitude from the point of the maximum slope after the initial sharp edge input [6], but they suffer from the difficulty in implementation and sensitivity to data processing. The method adopted in this paper is more straightforward, and accomplished by measuring the averaged pure time between control input (e.g. X_a) and the corresponding response (e.g. $\dot{p}$) as illustrated in Figure 7.

It is acknowledged that this estimating process involves the user's judgement subject to their experience, knowledge and expertise hence only an approximate value can be obtained. Another option would be to adopt the frequency-domain approach to estimate the time delay based on the phase-slope information [6], but this is beyond the scope of the method where we focus on the SID in the time domain.

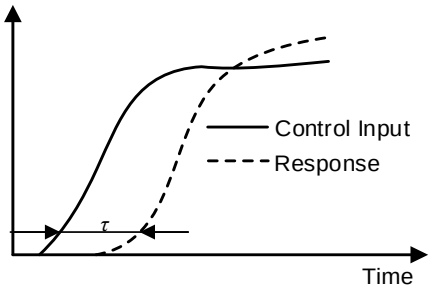

Figure 7 Illustration of estimating time delay

After obtaining the value of the time delay, the derivatives in Eq. (2) are estimated in sequence based on the activated timing point of the corresponding physical dynamics. The steps in the ASID approach are conducted using increasing amounts of dynamic response history and use a time-window approach. In the investigations reported in this paper, the left-hand edge of the window starts at the beginning of the time history. As the window is opened to the right, the first variable to be selected for fitting $\dot{p}$ is again that with the highest correlation. This is usually the control (consequently control derivative L_{Xa}), because it is activated before the rates build up. The value of L_{Xa} (and subsequent derivatives) is determined by the minimum value of the associated fit-error metric.

$$FitError = \frac{1}{T_j}\frac{\int_0^{T_j}(\dot{p} - \sum_{i=1}^{N} L_{x_i} x_i)^2 dt}{\int_0^{T_j} \dot{p}^2 dt} \quad (3)$$

in which x_i is the state/control variable and *N* is the number of identified derivatives (L_{x_i}), T_j the local period starting from the beginning used in the ASID at the j^{th} identification step. ASID then progresses through the $\dot{p}$ time history adding one or more variables (and associated derivatives) at a time to reduce the fit-error. The minimum fit-error value usually occurs at the same time as the derivative converges locally to a steady value. One or more candidate parameters in the proposed model structure (e.g., Eq. (2)) are identified using the primary response characteristic of the rotorcraft; others are then identified in a sequential manner.

The ASID approach is illustrated schematically in Figure 8. The ordering of variables x_i is determined by the sequence in which different physical dynamics are activated. The identified value Y_{xi} of a variable x_i is determined corresponding to the

minimum fit error at the timing point T_j. The left-hand edge of the analysis window remains at the initial time point and the right-hand edge opens to increase the window size. The least-squares fit-error for the specific force (normalised by the rotorcraft mass or moment of inertia), is integrated over the window size T_j in Eq. (3) which advances in steps, as more and more variables x_i are added, until the complete manoeuvre is modelled, or no further improvement can be achieved. Once identified in a specific time window, the derivatives stay fixed for the remainder of the manoeuvre and the ASID process.

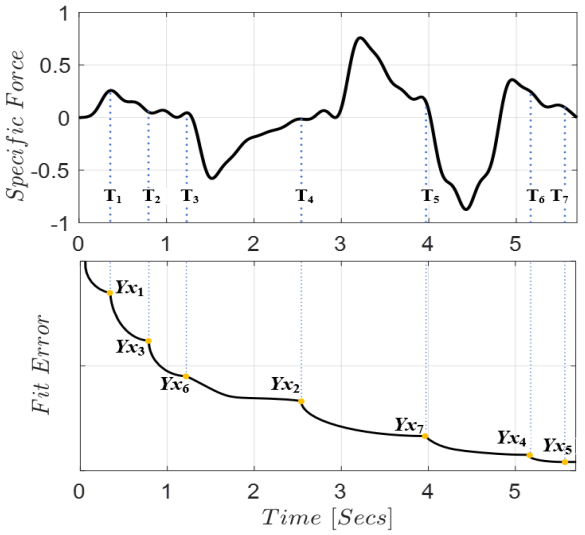

Figure 8. General approach to additive system identification

This feature of the ASID approach clearly differentiates it from the classical SID method in both time and frequency domains in terms of either EE or Output-Error (OE) analyses [10,21]. These conventional approaches process the complete time history at a time, so the identified derivatives are an average for the whole manoeuvre or, put in another way, the identified system shows average system behaviour [25]. The rationale behind the development of ASID is that a large part of the physics in the force contributions to a rotorcraft's motion should be 'identifiable' at the times when they are strongest. For example, the variable x_6 is identified at time T_3 and so on. Having clearly identified a force contribution, it can be fixed and not distorted later, perhaps to compensate for a mismatch occurring from an incorrect model structure. This assumes that linear, instantaneous approximations to the motion are valid of course. However, the method can also be applied to capture nonlinear and time-varying dynamics, as we shall explore.

The ASID approach is similar to recursive estimation methods [26,27] that are widely used for real-time SID in that the latter conduct the SID based on the data point by point when they become available. However, these recursive estimation methods have no mechanism applied to judge the sequence of derivatives to be identified based on the physical information in the way that ASID does. Moreover, the number of derivatives is typically fixed during the recursive SID process but in the ASID method, this is variable.

3.3. Results of ASID applied to Nlr F-B412

To demonstrate the effectiveness of the ASID method, we use the Nlr F-B412 (w/o MWD) responses at hover as shown in Figure 9. The first step is to identify the equivalent time constant for the higher-order dynamics. For example, the roll-regressing-flap mode, can be approximated with the shaft-fixed flapping response model [24] as

$$\tau_f \dot{\beta}_{1s} = -\beta_{1s} + \tau_f p + \theta_{1c} \tag{4}$$

where τ_f is the rotor flap time constant, θ_{1c} is the blade cyclic pitch and β_{1s} is the lateral cyclic flapping. The identified τ_f value of about 0.1sec is shown to have converged after about 0.3sec in Figure 10. The circles in the middle plot represent each segment (from zero to the current timing point) used for ASID to derive each corresponding values of squares in the Figure 10.

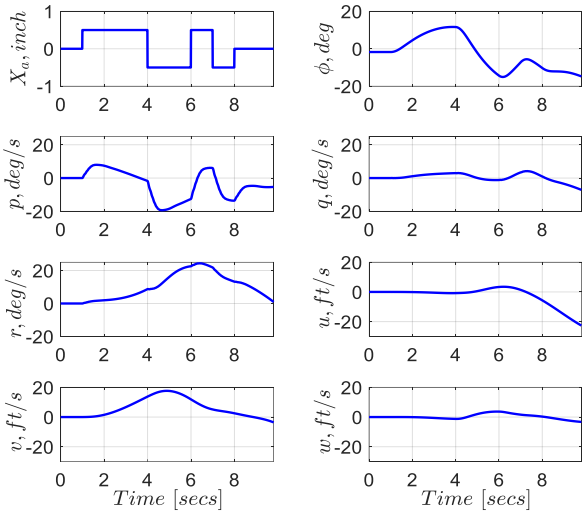

Figure 9 Responses of Nlr F-B412 (w/o MWD) at hover with a 3211 lateral stick input

With the ASID method, the derivatives are estimated in sequence. The control derivative L_{Xa} is the first derivative chosen for identification. This is physically understandable since after applying the lateral stick input, the rotor disk re-orientates rapidly due to the flapping dynamics (τ_f = 0.1sec), producing a roll moment and leading to the fuselage roll motion building up. As shown in Figure 9, the roll rate increases after the control is applied. The period used for identifying L_{Xa} value should be

as short as possible to reduce the level of the roll rate contribution. Therefore, a very short time window (0.1sec) is chosen for ASID as shown in Figure 11 and the L_{Xa} value is determined to be 0.897, within the window between 1.05 and 1.08sec.

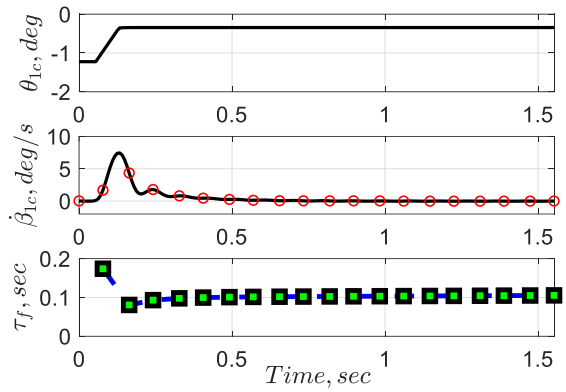

Figure 10 ASID results for τ_f using a step input

Figure 9 shows that there is negligible surge u velocity and very little sway velocity v (≈ 2 ft/s) up to 2sec. The heave velocity is very small during the whole manoeuvre. Meanwhile, both pitch and yaw rates are less than 0.86 deg/s at 2sec. The roll rate is dominant between 1.1 and 2sec. Furthermore, this can be physically understood in terms of the fuselage motion building up rapidly following the rotor disk tilting. Taking these factors into consideration, L_p is selected as the second derivative.

After 1.8sec, both the sway velocity and pitch rate are increasing. Although the former increases fairly rapidly after 2sec, it contributes to $\dot{p}$ over a similar time as q. Therefore, L_v and L_q are combined for the identification in the next window. As shown in Figure 12, these derivative estimates are fairly constant between 3 and 4sec. L_w is the fourth derivative chosen for identification due to the heave velocity beginning to contribute at around 3.8sec. However, the quality of this estimate is degraded due to the very small amplitude of heave response (hence less significant to $\dot{p}$).

L_r is the fifth derivative and it deserves more comment due to its complex pattern. The yaw rate builds up early on as shown in Figure 9, due to the roll-yaw coupling excited by $\dot{p}$ with a non-zero product of inertia, I_{xz}. Moreover, it is small until the sway velocity builds up at about 3sec. Therefore, these factors may degrade the quality of the L_r identification. Finally, L_u is chosen as the sixth derivative. In Table 1, the derivatives computed using ASID are compared with the small perturbation values from the F-B412 linearisation process.

The responses with the two derivative sets in Table 1 are compared with $\dot{p}$ of the Nlr F-B412 in Figure 13; the oscillations likely stemming from higher-order dynamics, including the (2/rev) lead-lag motion. The 6DoF model structure described in Eq. (2) is not able to capture these oscillations that are considered as process noise in the SID. However, they certainly will increase the fit error. It can be seen in Figure 13 that the fit of the perturbation derivative model is the poorest. The ASID results are superior to the perturbation model, and it may be that the translational velocities have an impact on these differences.

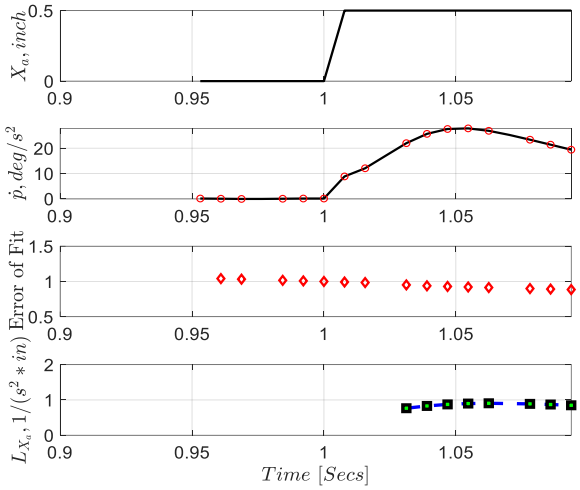

Figure 11 SID results for L_{Xa} using the ASID approach

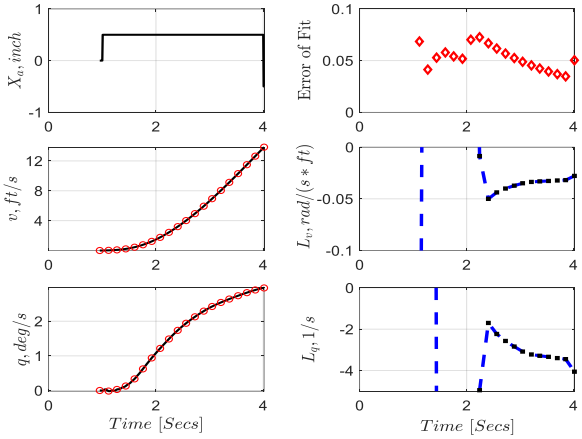

Figure 12 SID results for L_v and L_q using ASID approach

Table 1 Derivative Comparisons between ASID and perturbation analysis obtained from Nlr F-B412 (w/o MWD) with 3211 multi-step lateral stick input at hover (arranged in order of selection)

Derivatives	ASID	Pert. Values
L_{Xa}	0.897	0.893
L_p	-2.95	-3.163
L_q	-3.54	-2.492
L_v	-0.031	-0.031
L_w	0.013	-0.004
L_r	0.320	0.014
L_u	0.034	0.030

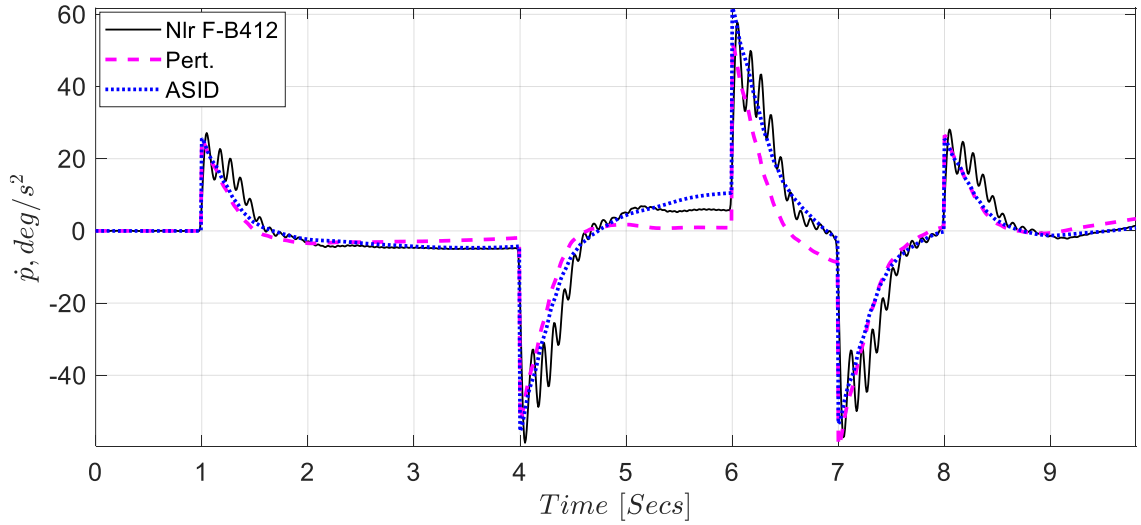

Figure 13 Comparison of $\dot{p}$ with linear models derived with ASID and perturbation analyses

3.4. ASID with Flight Test Data

In this section, ASID is applied to the B-412 FT data at hover and is extended from the roll dynamics in Eq. (5) to the 4DoF state-space model (*X, Y, L, M*), with the structure given in Eq. (5). The heave (*w*) and yaw (*r*) dynamics are not included in these model structures, based on the argument that they are only loosely coupled with the roll and pitch motions in hover.

$$
\begin{aligned}
\dot{u} &\approx X_{X_b} X_b(t-\tau_{x_b\dot{u}}) + X_{X_a} X_a(t-\tau_{x_a\dot{u}}) + X_u u \ldots \\
&\quad + X_q q + X_v v + X_p p - g\theta \\
\dot{q} &\approx M_{X_b} X_b(t-\tau_{x_b\dot{q}}) + M_{X_a} X_a(t-\tau_{x_a\dot{q}}) + M_u u \ldots \\
&\quad + M_q q + M_v v + M_p p \\
\dot{\theta} &\approx q \\
\dot{v} &\approx Y_{X_b} X_b(t-\tau_{x_b\dot{v}}) + Y_{X_a} X_a(t-\tau_{x_a\dot{v}}) \ldots \\
&\quad + Y_u u + Y_q q + Y_v v + Y_p p + g\phi \\
\dot{p} &\approx L_{X_b} X_b(t-\tau_{x_b\dot{p}}) + L_{X_a} X_a(t-\tau_{x_a\dot{p}}) + L_u u \ldots \\
&\quad + L_q q + L_v v + L_p p \\
\dot{\phi} &\approx p
\end{aligned}
\qquad (5)
$$

Angular accelerations are derived from the rate measurements through first-order differentiation. Translational accelerations have been derived from the corresponding accelerometer measurements. A low-pass filter with 3Hz cut-off frequency has been implemented to smooth the FT data for both input and output responses.

The stability and control (perturbation) derivatives of the F-B412 model in hover are included in Table 2 and 3, respectively. The derivatives computed using the ASID approach are shown in Table 4 and Table 5. The time point values in Table 6 show the moments when the contribution from the derivatives are chosen. All the control derivatives are chosen as the first candidate in the ASID.

Table 2 Stability derivatives of 4DoF linear F-B412 model using perturbation method

	u	*q*	*v*	*p*
X	-0.013	0.682	-0.010	0.497
M	0.004	-0.510	0.005	-0.360
Y	0.013	1.315	-0.032	-0.766
L	0.031	4.491	-0.033	-3.312

Table 3 Control derivatives of 4DoF linear F-B412 model using perturbation method

	X_a	X_b
X	0.083	0.718
M	-0.030	-0.205
Y	0.474	-0.140
L	0.910	-0.354

Table 4 Stability derivatives of 4DoF linear FT model using ASID method (hover)

	u	*q*	*v*	*p*
X	-0.035 (4)	5.846 (2)	0.347 (5)	-0.477 (3)
M	0.006 (3)	-0.509 (2)	0.005 (5)	-0.267 (4)
Y	-0.002 (5)	1.457 (4)	-0.209 (3)	-0.200 (2)
L	0.056 (5)	0.367 (3)	-0.050 (4)	-2.780 (2)

Table 5 Control derivatives of 4DoF linear FT model using ASID method (hover)

	X_a	X_b	τ_{xa}	τ_{xb}
X	0.343	1.277	0.08	0.14
M	-0.044	-0.220	0.05	0.12
Y	1.108	-0.933	0.17	0.14
L	1.027	-0.224	0.14	0.14

Table 6 Time points (seconds) when the derivative(s) are chosen using ASID method (FT, hover)

	u	*q*	*v*	*p*	X_a	X_b
X	1.45	1.25	3.57	1.34	0.58	0.47
M	2.31	1.26	4.49	3.37	0.47	0.45
Y	3.87	3.72	3.01	1.03	0.38	0.41
L	3.86	1.10	2.88	0.86	0.40	0.43

The following points can be drawn from the derivative tables above. Firstly, considering the first two steps in the ASID process, there is a reasonable agreement for the values of the key (on-axis) damping and control derivatives between the ASID and perturbation values in the pitch and roll axes. Secondly, there are larger differences among the off-axis derivatives, particularly L_q, although many of the force derivatives are small in hover and low speed.

The large contribution of the FLIGHTLAB MWD effect to the cross-damping derivative L_q was discussed earlier and is further investigated later in the paper. The speed stability derivative M_u is 50% higher in FT, implying a slightly more unstable hover phugoid, as indicated in Figure 14, in which the eigenvalues of both sources are compared. The roll and pitch subsidence are quite close and the Dutch roll mode from FT will be degraded due to the absence of the yaw dynamics in the ASID model.

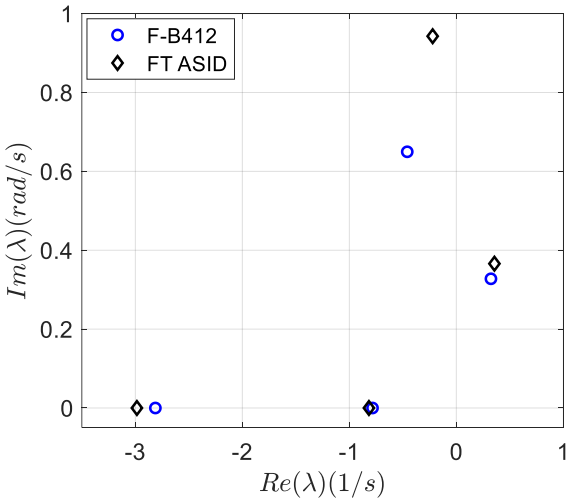

Figure 14 Comparison of eigenvalues using ASID and perturbation derivatives

As shown in Figure 15 and Figure 16, the two, on-axis, derivatives for each case capture most of the fit error in the ASID model, which reduces further as the speed stability derivative, M_u, or the dihedral effect, L_v, enter into the model structures. The remaining derivatives make very small contributions to the fit errors. This is reflected in Figure 17 and Figure 18 in which the significance level of each component contribution to the overall $\dot{p}$ and $\dot{q}$ response is illustrated by reconstructing the dynamics using the identified components.

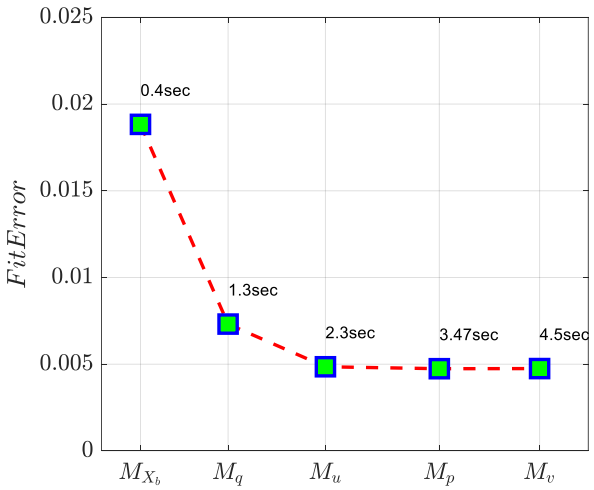

Figure 15 The fit-error varying as the different contributions to the dynamics are added in the ASID process ($\dot{q}$ response)

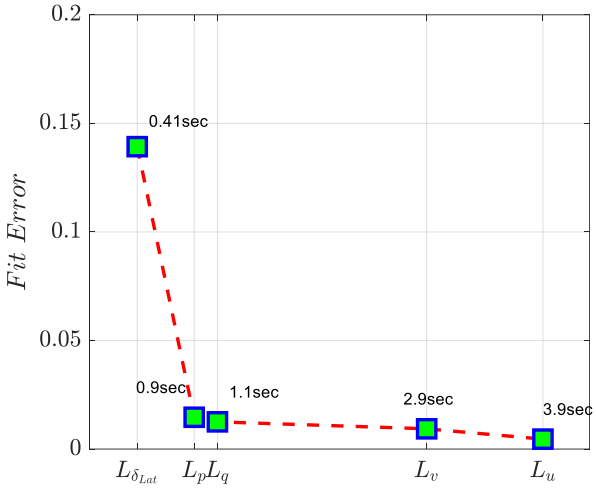

Figure 16 The fit-error varying as the different contributions to the dynamics are added in the ASID process ($\dot{p}$ response)

In accordance with Figure 16, the reconstructed roll response in Figure 17 has reached a good agreement with FT after only L_{Xa} and L_p components are introduced. The fit is improved when the dihedral stability derivative L_v shows its effects after 1.5sec, and is further improved when L_u plays its role at 2sec. The latter also significantly improves the fit after 5sec. Despite the relatively early selection of pitch rate q, the moment L_qq hardly affects the fit. Similar findings in the $\dot{q}$ response are shown in Figure 18.

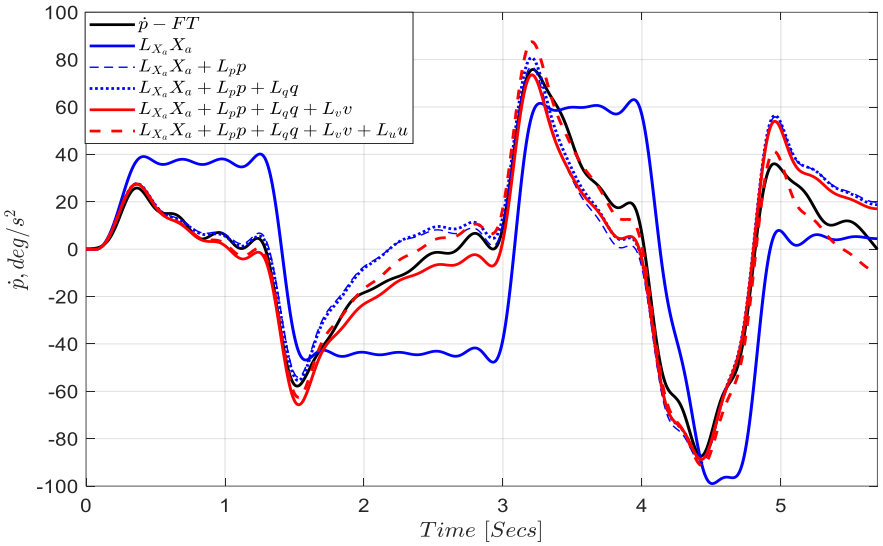

Figure 17 Reconstructing the dynamics using the identified derivatives ($\dot{p}$ response)

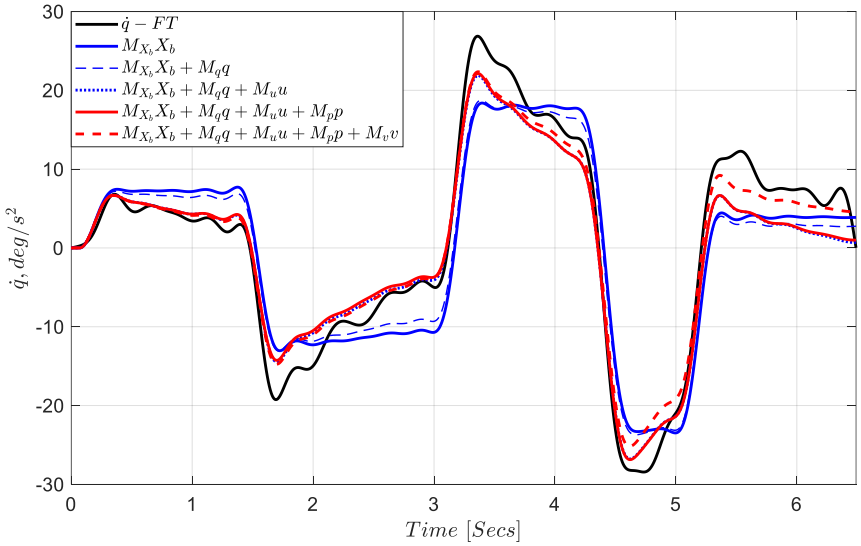

Figure 18 Reconstructing the dynamics using the identified derivatives ($\dot{q}$ response)

Both these figures, effectively motion signatures (MoSis), reveal contributions from the various aircraft motions to the total acceleration. Furthermore, the quality of the derivatives in Table 4 and Table 5 can be demonstrated with FT and the Nlr F-B412 with MWD by comparing their reconstructed MoSis (e.g. $\dot{q}$ and $\dot{v}$) using Eq. (5), as shown in Figure 19. As before, the results in these figures are derived and filtered from the measurements through first-order differentiation (3Hz bandwidth).

The comparisons in Figure 19 show a generally good match between the three sources in the $\dot{q}$, $\dot{p}$ and $\dot{v}$ response. The high frequency oscillations in $\dot{u}$ response (FT) are from two possible sources: noise in the measured FT inertial accelerations (used to derive the body velocity u) and the numerical differential process (from u to $\dot{u}$). It is acknowledged that these 'unrealistic' oscillations may contaminate the process of identifying X_{Xb} using AISD. The initial $\dot{u}$ of ASID is larger than Nlr F-B412, reflecting the larger X_{Xb}. After 2sec, the fit of ASID with FT is better than the Nlr F-B412 in the $\dot{u}$ response. A similar explanation can be given for the $\dot{v}$ response within the first second. ASID also achieved improved results over the Nlr F-B412 in the $\dot{p}$ response but is slightly inferior in $\dot{q}$.

These comparisons not only highlight the accuracy of the identified ASID model, but also demonstrate a reasonable fidelity of the longitudinal and lateral responses of the Nlr F-B412 with MWD, when viewed in MoSi form. However, this does not mean the individual contribution of each derivative in the response match their corresponding FT data; in fact, the differences can be quite significant, for example, as reflected in Figure 20 where the breakdown of contributions is shown.

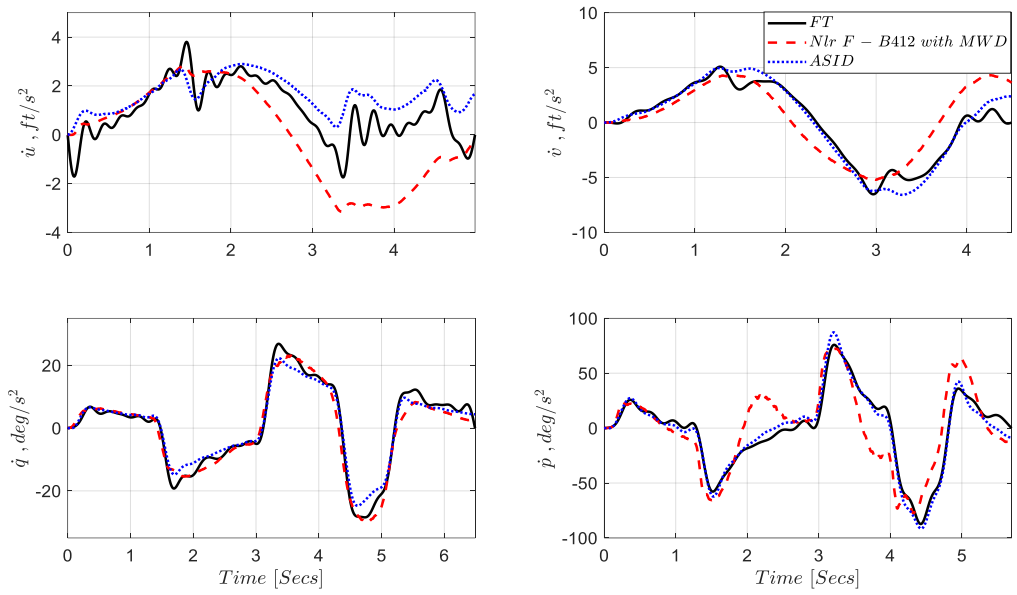

Figure 19 Comparison of fit across three sources: FT, Nlr F-B412 with MWD, and ASID

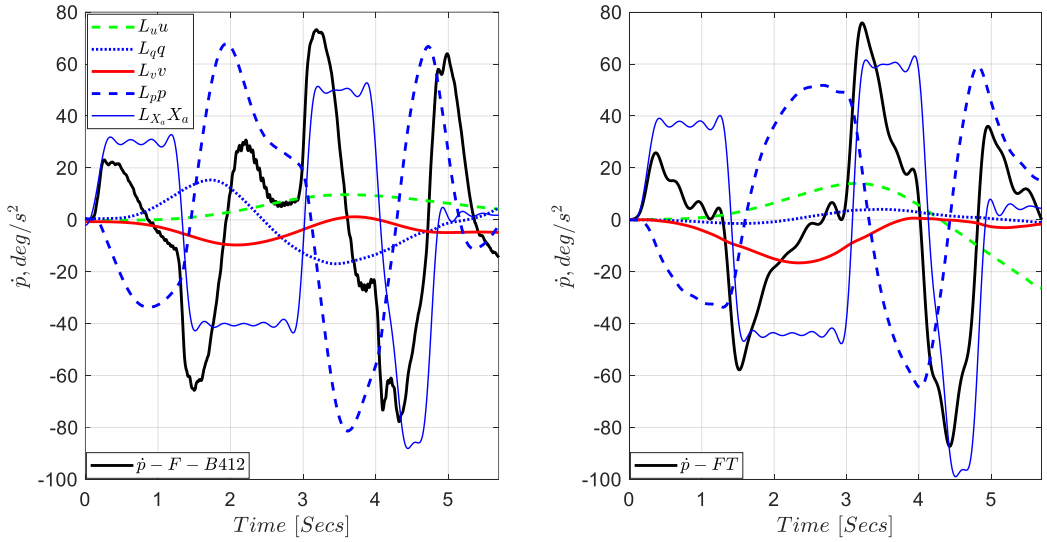

Figure 20 Comparison of the contributions of individual components to $\dot{p}$ (Left, F-B412 and Right, FT)

The moments due to control and roll rate to the overall $\dot{p}$ have a similar pattern of variation and amplitudes between Nlr F-B412 and FT. As shown in Figure 20, the major difference lies in the derivatives L_q and L_v. L_q has earlier and larger contributions for the F-B412. L_u always has a positive contribution in the F-B412 but in the FT ASID model it quickly drops down at 3sec and then becomes negative after 4sec. This is reflected in the real aircraft having a more rapid and larger pitch up response as shown in Figure 21.

The differences across the two methods can be beneficial to revealing the potential deficiencies of the physical source in the modelling errors and indicate how these deficiencies might be repaired by making use of the information from FT data through the ASID approach. This will be a focus in the next steps of the research. The F-B412 results have already been shown in Figure 6. The ASID model roll response following the lateral cyclic input matches the FT results very closely. The off-axis pitch response is about 50% of that in flight. The cross-damping derivative L_q was estimated very early in the manoeuvre, and it is suspected that MWD effects continue to evolve as the manoeuvre progresses; a nonlinear evolution that the current linear model does not capture.

Following the longitudinal control input, the pitch response from ASID departs from FT after about 4sec. The off-axis roll response matches reasonably well with flight through the manoeuvre. However, the translational velocities from the ASID model do not compare well with FT. This is attributed to the poor estimates of the X and Y derivatives in Eq. (5), already discussed from the comparisons in Figure 6.

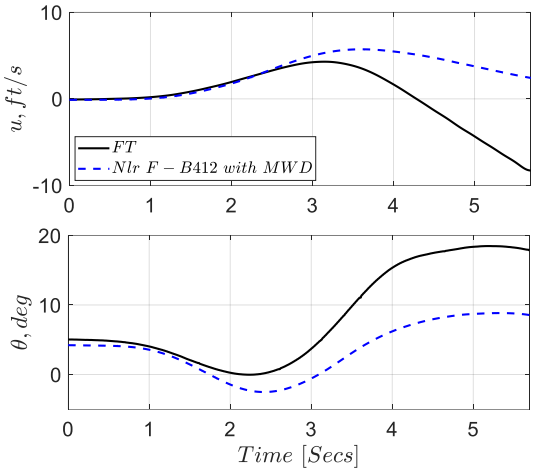

Figure 21 Comparison of surge velocity and pitch attitude response between Nlr F-B412 with MWD and FT (lateral input)

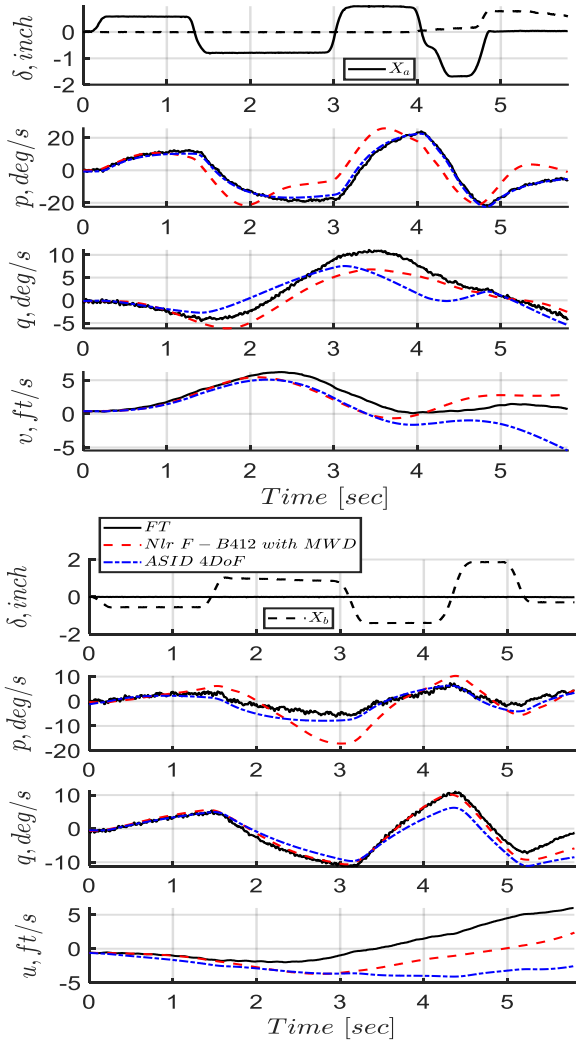

Figure 22 Validation study using the alternate test data: Comparison of responses from the ASID 4DoF linear model with FT and Nlr F-B412 with MWD

The validation results of the ASID process are shown in Figure 22 where the response comparisons are shown for a different test case than used for the identification of derivatives. Similar results as those in Figure 23 have been achieved here but, the linear ASID model pitch response matches more closely with FT with a lateral cyclic input for about 3sec. All these results have demonstrated the good fidelity of Nlr F-B412 in both the *p* and *q* channels as well as the 4DoF ASID results.

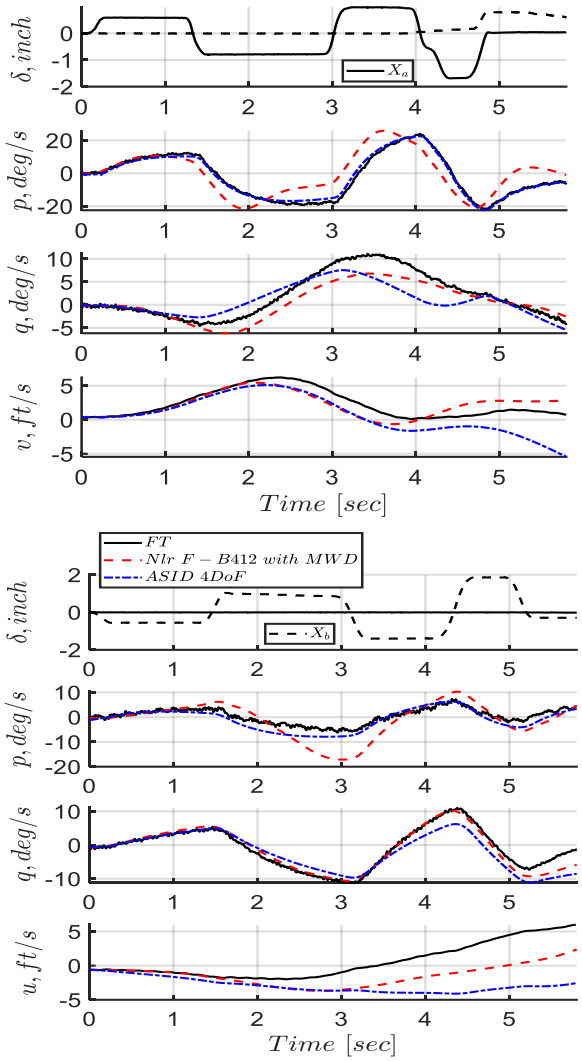

Figure 23 Verification study using the SID test case data: Comparison of responses from the ASID 4DoF linear model with FT and Nlr F-B412 with MWD

The results of the ASID analysis presented above are encouraging. Physical effects are captured as they occur and then fixed, not requiring further adjustments to compensate for modelling deficiencies encapsulated in average derivatives. The potential nonlinearities will now be explored.

4. EXPLORING NONLINEARITY WITH ASID

In Section 2, the investigation showed that the nonlinearity arising from the cubic roll rate in Eq.

(1) degrades identifiability in the frequency domain. ASID is applied to the responses of the three cases (with k_p = 0, 1, and 2) to estimate L_p and k_p values and the results are compared with those from the frequency domain SID approach in Table 7. In particular, the ASID procedure for Case 2 is illustrated in Figure 24 to show the influence of the nonlinearities on the SID process.

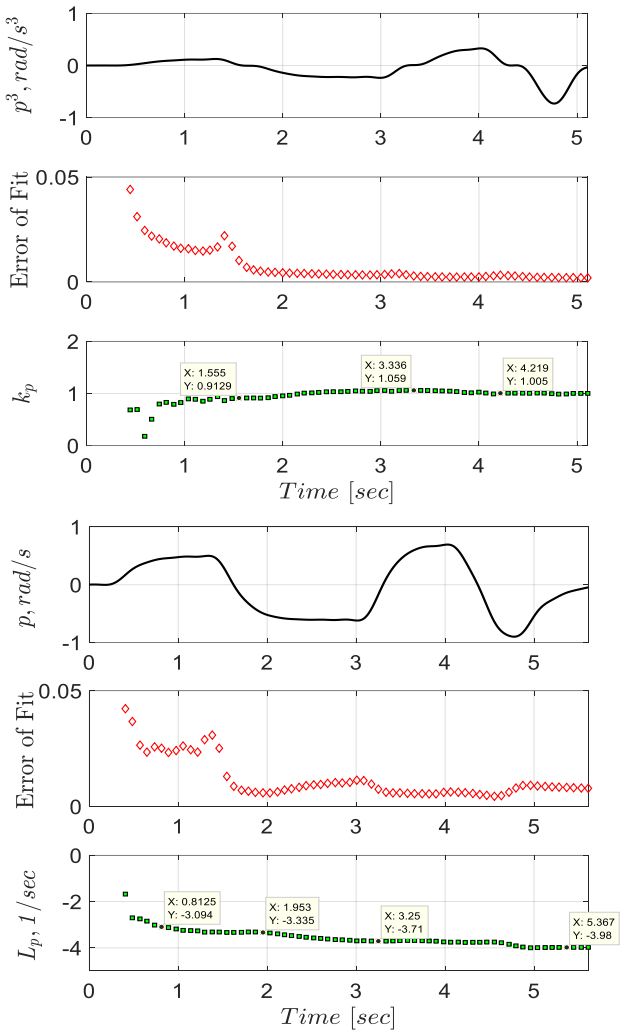

Figure 24 Illustration of the influence of nonlinearities on ASID to derive L_p (Step 2) and k_p values (Step 3)

Table 7 Comparison identified parameters from ASID and frequency domain methods

	Case	L_{Xa}	L_p	k_p
ASID	1	0.865	-2.748	0.027
	2	0.865	-3.094	1.036
	3	0.865	-2.906	1.979
Freq. Method	1	0.946	-3.199	--
	2	0.862	-4.010	--
	3	0.888	-4.955	--

A 3Hz low-pass filter was implemented to smooth the data for the ASID analysis. The frequency-domain approach adopted the 1DoF linear model structure. The L_{Xa} values in Table 7 obtained using ASID in Step 1 are same for all the three cases; 3% different from the true value of 0.896. This is reasonable since the nonlinear term will only physically start to play the role after the initial roll acceleration that is directly connected with the applied input. Moreover, the amplitude of p is about 7 times larger than p^3 when t < 1sec (10 times t < 0.5 sec) as shown in Figure 24. Therefore, it is logical to conclude that p is dominant when t < 1 sec and the 1DoF roll model can be validated in this period, where the response is essentially linear. This results in similar L_p values at Step 2 (the inverse of $t_{63\%}$) across the three cases and these are identified at 0.81 sec, corresponding to the minimum fit-error in this period. After L_{Xa} and L_p are obtained, the k_p values can be derived in Step 3 (as illustrated in Figure 24 for Case 2); all three are close to the true values as shown in Table 7.

The L_{Xa} results from the frequency-domain approach are close to the true values. However, L_p is contaminated by the nonlinearities, since these values are averaged across the whole manoeuvre. This is why, for example, L_p from Case 2 is -4.010, almost the same as the final value (-3.982) in Figure 24, when all data are used in the ASID. However, Figure 24 shows L_p varying across the manoeuvre due to the nonlinearity. Here it is acknowledged that the Linear Regression approach can obtain all these three values in one step since there is no extra noise. However, the purpose here is to show the ASID as a powerful tool to dissect the influence of the nonlinearities as their influence grows in a manoeuvre.

Now the research moves to explore the nonlinear effects arising from large amplitude responses of a nonlinear system excited by different levels of control input. The lateral step responses of the Nlr F-B412 with MWD with four levels of pulse input size are shown in Figure 25.

For this analysis, the maximum input size is determined by the criteria that the corresponding roll attitude is about 30deg. Such a large pulse might be applied for example during quickness testing for handling qualities assessments. In this study, the large inputs are purposely applied to excite any nonlinearities that cannot be captured accurately by a conventional linear analysis only valid within a small region around the trim condition. The large input size is expected to violate this condition and, therefore, enable exploration of any nonlinearities in a flight system.

The following linear model structure is adopted for the initial investigation.

$$\dot{p} = L_{X_a} X_a + L_p p + L_q q + L_v v \qquad (6)$$

Compared with Eq. (5), L_u is ignored due to its minor contribution, reflected in the small fit error change in Figure 16. ASID is applied to the Nlr F-B412 with MWD using Eq. (6) for the responses with 4 input sizes in Figure 25. The results are shown in Figure 26.

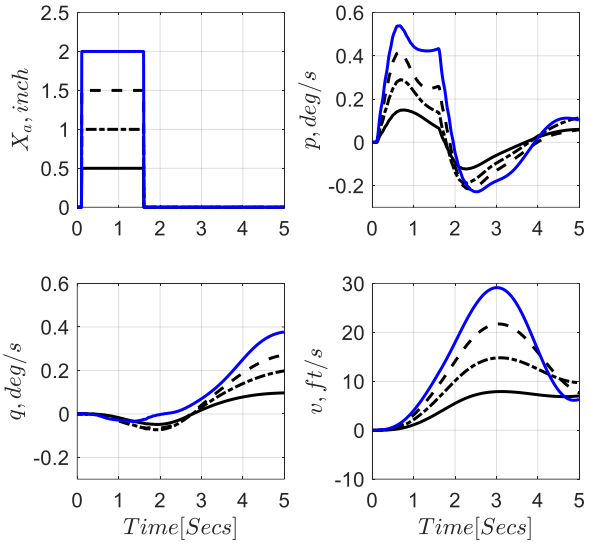

Figure 25 Response of Nlr F-B412 (with MWD) for different levels of lateral pulse control input (pulse width 1.5 sec)

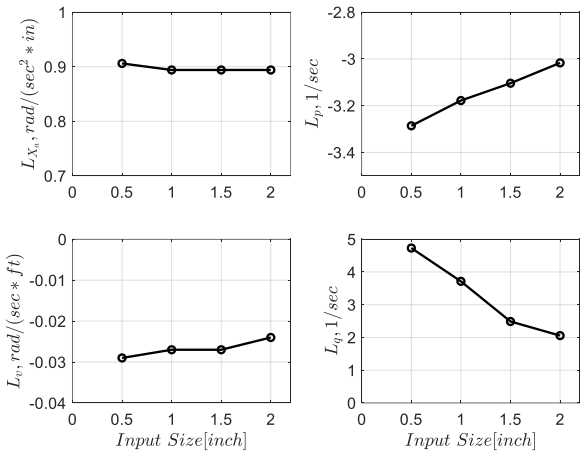

Figure 26 Derivative variations vs step input size using ASID

The control derivative L_{Xa} is almost constant with different levels of a control step size. This is reasonable as L_{Xa} is identified in the initial very-short time period using the ASID in which the nonlinearities are yet to develop. L_q shows significant change indicating strong sensitivity of this aerodynamic effect as it develops [28]. L_p decreases by about 10% as the input size increases. L_v shares the similar decreasing pattern as L_p but with smaller magnitude. To capture the nonlinearities associated with L_q, attributed to the MWD effect, the following equation is proposed,

$$\dot{p} = L_{X_a} X_a + L_p p + L_v v + L_q q(1 + k_q q^2) \qquad (7)$$

in which k_q and the related cubic q represent the nonlinear dynamics. After fixing L_{Xa} (0.90), L_p (-3.15), L_v (-0.031), and L_q (3.076), from Figure 26 using the responses in Figure 25, the k_q value is found to be -16.16, reflecting a strong supressing nonlinear effect. The predictability of these values is demonstrated in Figure 27. For the three levels of doublet input shown in Figure 27 and Figure 28, the responses of the nonlinear model in Eq. (7) have reached a good agreement with the responses of the Nlr F-B412.

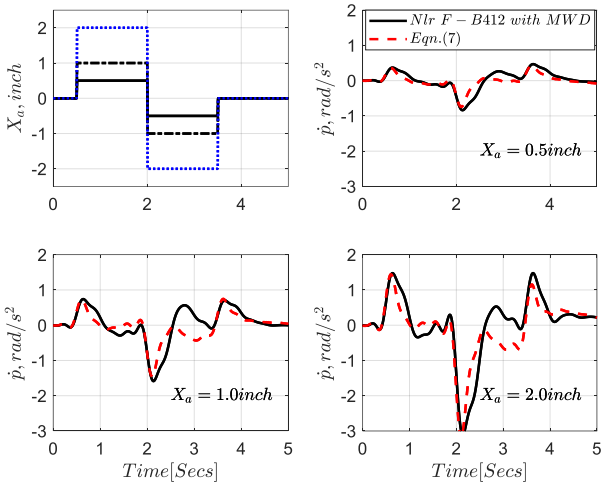

Figure 27 Response comparison of Eq.(7) with the Nlr F-B412 with MWD (roll acceleration, Doublet input)

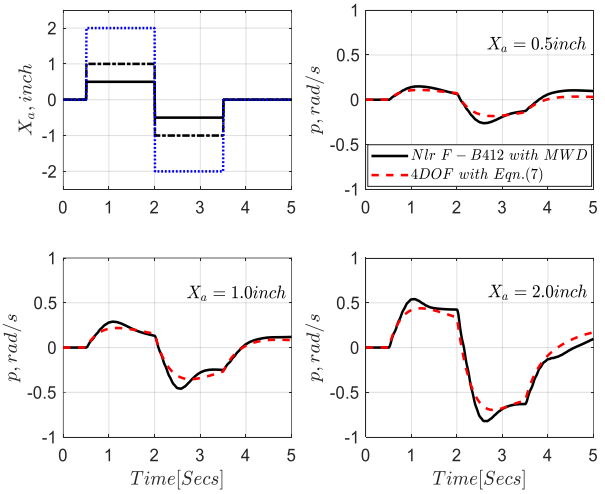

Figure 28 Response of Nlr F-B412 (with MWD), compared with the 4DoF model with modified $\dot{p}$ using Eq.(7) (roll rate, Doublet input)

The 4DoF model fails to capture the overshoot seen in the Nlr Model around 1 sec, likely due to the impact of flap dynamics in the full state nonlinear model. These results suggest a degree of validation of this model structure and associated identified coefficients for capturing the key

nonlinear character of MWD. It is argued that, as the response amplitude builds up, the MWD effect reduces in magnitude as the wake spreads and skews 'downstream', evident in both the short and long term *q* response in Figure 25. This hypothesis needs to be put to stronger tests than presented in this paper and will be the subject of the ongoing research.

5. CONCLUSIONS AND NEXT STEPS

The paper reports progress in the development of a new approach to the exploration of rotorcraft simulation fidelity, referred to as Additive System Identification (ASID), for application to low-speed manoeuvres. The approach is based in the time domain and captures the contributions from controls and motions to forces and moments 'additively', as a response evolves following control inputs. In previous research the authors have captured contributions, identifying stability and control derivatives, in the frequency domain, to create linear models suitable for stability analysis of rotorcraft in forward-flight trim conditions. For the present investigation, flight test data gathered with the NRC's Bell 412 ASRA in-flight simulator have been compared with responses from the FLIGHTLAB model of the aircraft, the F-B412. Results are presented for tests conducted in the hover with 2311 multi-step inputs in pitch and roll. From the analysis undertaken, the following conclusions and observations can be drawn.

- The ASID approach has proved effective at identifying the primary motion and control derivatives following control inputs at hover, confirmed by the resulting good matches with flight test data.
- The fidelity of the baseline F-B412 is shown to be reasonably good, particularly with the manoeuvre wake distortion (MWD) effects included, that serve to reverse the cross-damping effects and the associated derivatives, L_q and M_p.
- Motion Signatures (MoSis) are useful for revealing the contributions of the various motions and controls to the overall forces and moments. Similar levels of comparison with test data can be achieved with different combinations of motions, and this can be used to explore fidelity deficiencies in the simulation model.
- Nonlinearities excited by large pulse inputs have shown a significant effect on the MWD derivative L_q but less on L_v and L_p. A nonlinear term has been introduced to model effects associated with L_q. It is hypothesised that this is caused by reducing MWD effects as the wake develops from the hover condition.

The research has presented encouraging results but more needs to be done. The multi-DoF ASID approach based on Output-Error analysis is under development for capturing inter-coupling couplings. ASID will also be applied more extensively to the pitch dynamics to capture the nonlinearities and hysteretic effects caused by rotor-wake interference on the fuselage and empennage. Integration of ASID with the renovation methodology previous reported is underway and will feature in future publications.

6. ACKNOWLEDGEMENTS

The UK authors acknowledge the funding support from the Engineering and Physical Sciences Research Council for the RSF project under grant numbers EP/P031277/1 and EP/P030009/1. Contributions from staff at the Canadian NRC are acknowledged, particularly the ASRA facility manager, Bill Gubbels. The authors also thank Dr Chengjian He of Advanced Rotorcraft Technology Inc. for the image of the rotor wake shown in Figure 1. The reported research is also contributing to the NATO STO AVT-296 activity, '*Rotorcraft flight simulation model fidelity improvement and assessment*'.

APPENDIX

The stability and control derivatives of F-B412 model varying with forward speed are shown in this Appendix.

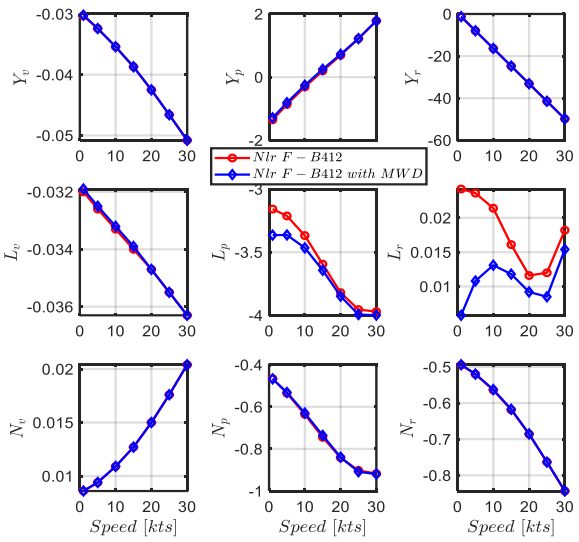

Figure A.1 Lateral stability derivative of F-B412

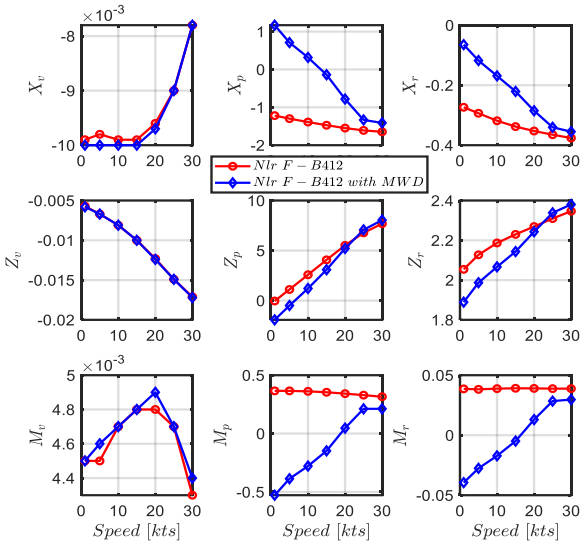

Figure A.2 Longitudinal stability derivative of F-B412

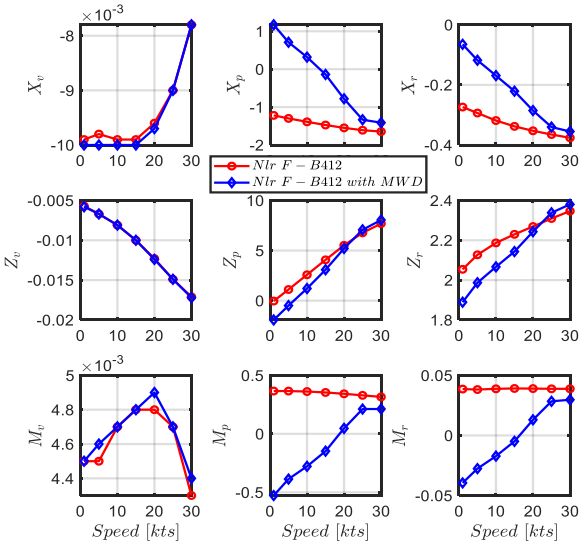

Figure A.3 Longitudinal to lateral stability derivative of F-B412

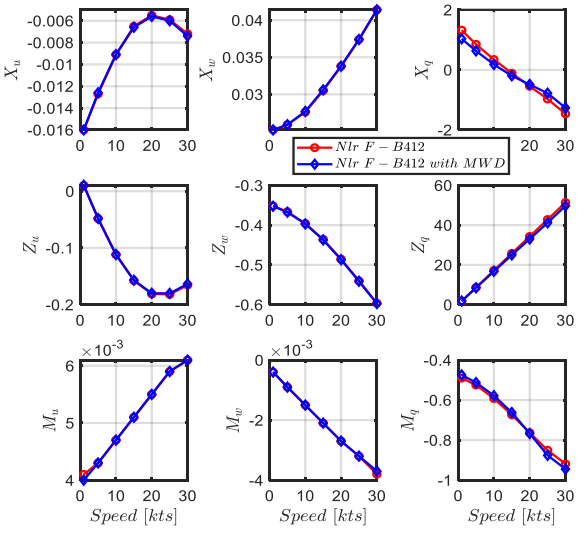

Figure A.4 Lateral to longitudinal stability derivative of F-B412

References

[1]. Anon, *Certification Specifications for Helicopter Flight Simulation Training Devices, CS-FSTD(H),* EASA, Initial issue, 26 June 2012.

[2]. Anon, FAA 14 Part 60 Flight Simulation Training Device Initial and Continuing Qualification and Use, Appendix C to Part 60-Qualification Performance Standards for Helicopter Full Flight Simulators, 2016.

[3]. Tischler M.B., Remple R.K., *Aircraft and Rotorcraft System Identification: Engineering Methods with Flight-test Examples,* American Institute of Aeronautics and Astronautics, 2006.

[4]. Lu L., Padfield G.D., White M.D., Perfect P., Fidelity Enhancement of a Rotorcraft Simulation Model through System Identification. *The Aeronautical Journal,* vol. 115, no. 1170, pp 453-470, 2011.

[5]. Drobik J.S., Brian G.J., Application of System Identification Techniques to the F-111C and PC 9/A Aircraft. *J Aircraft,* vol. 41, no. 4, pp 744-751, 2004.

[6]. Morelli E.A., Klein V., "Application of System Identification to Aircraft at NASA Langley Research Center". *J Aircraft,* vol. 42, no. 1, pp 12-25, 2005.

[7]. Klein V., Morelli E.A., *Aircraft System Identification: Theory and Practice,* American Institute of Aeronautics and Astronautics Reston, VA, 2006.

[8]. Padfield G.D., Thorne R., Murray-Smith D., Black C., Caldwell A.E., UK Research into System Identification for Helicopter Flight Mechanics. *Vertica,* vol. 11, no. 4, pp 665-684, 1987.

[9]. Hamel P.G., Kaletka J., Advances in Rotorcraft System Identification. *Prog Aerospace Sci,* vol. 33, no. 3-4, pp 259-284, 1997.

[10]. Tischler M.B., Remple R.K., *Aircraft and Rotorcraft System Identification,* 2nd Ed. AIAA, 2012.

[11]. Wei W., Cohen K., Tischler M.B., System Identification and Controller Optimization of a Quadrotor UAV, Proceedings of the 71st Annual Forum of the American Helicopter Society, Virginia Beach, VA, May 5-7, 2015.

[12]. Vitale A., Genito N., Federico L., Corraro F., Hybrid Approach for Rotorcraft Identification from Flight Data, Proceedings of the 67th Annual Forum of the American Helicopter Society, Virginia Beach, VA, May 3-5, 2011.

[13]. Spira D., Myrand-Lapierre V., Soucy O., Reducing Blade Element Model Configuration Data Requirements using System Identification and Optimization, Proceedings of the 68th Annual Forum of the American Helicopter Society, Fort Worth, Texas, May 1-3, 2012.

[14]. Seher-Weiss S., Greiser S., Wartmann J., Gubbels A.W., Ricciardi J., Hui K., Bell 412 System Identification: Comparing Methods and Tools, Proceedings of the 75th Annual Forum of the

American Helicopter Society, Philadelphia, PA, May 12-16, 2019.
[15]. Greiser S., Grünhagen W., Improving System Identification Results: Combining a Physics-Based Stitched Model with Transfer Function Models Obtained Through Inverse Simulation, Proceedings of the 72nd Annual Forum of the American Helicopter Society, West Palm Beach, Florida, May 17-19, 2016.
[16]. Geluardi S., Nieuwenhuizen F.M., Pollini L., Bülthoff H.H., Frequency Domain System Identification of a Light Helicopter in Hover, Proceedings of the 70th Annual Forum of the American Helicopter Society, Montreal, Canada, May 20-22, 2014.
[17]. Cameron N., White M.D., Padfield G.D., Lu L., Agarwal D., Gubbels A.W., Rotorcraft Modelling Renovation for Improved Fidelity, 75th Annual Forum & Technology Display, Philadelphia, USA, May 13-16, 2019.
[18]. Du Val R.W., He C., Validation of the FLIGHTLAB Virtual Engineering Toolset. *The Aeronautical Journal,* vol. 122, no. 1250, pp 519-555, 2018.
[19]. White M.D., Lu L., Padfield G.D., Gubbels A.W., Cameron N., *A Novel Approach to Rotorcraft Simulation Fidelity Enhancement and Assessment,* 2017, https://www.researchgate.net/project/A-Novel-Approach-to-Rotorcraft-Simulation-Fidelity-Enhancement-and-Assessment.
[20]. He C., Zhao J., Modeling Rotor Wake Dynamics with Viscous Vortex Particle Method. *AIAA J,* vol. 47, no. 4, pp 902-915, 2009.
[21]. Morelli E.A., Klein V., *Aircraft System Identification: Theory and Practice,* 2nd Ed. Sunflyte Enterprises Williamsburg, VA, 2016.
[22]. Peters D.A., He C.J., Finite State Induced Flow Models. II-Three-Dimensional Rotor Disk. *J Aircr,* vol. 32, no. 2, pp 323-333, 1995.
[23]. Zhao J.. Dynamic wake distortion model for helicopter maneuvering flight, PhD thesis, 2005.
[24]. Padfield G.D., *Helicopter Flight Dynamics: Including a Treatment of Tiltrotor Aircraft,* Third Ed. John Wiley & Sons, 2018.
[25]. Jategaonkar R.V., *Flight Vehicle System Identification: A Time-Domain Methodology,* American Institute of Aeronautics and Astronautics, Inc., 2015.
[26]. Ljung L., Söderström T., *Theory and Practice of Recursive Identification,* MIT Press, 1983.
[27]. Haykin S.S., *Adaptive Filter theory,* Prentice-Hall, Inc., 1986.
[28]. Keller J.D., An Investigation of Helicopter Dynamic Coupling using an Analytical Model. *Journal of the American Helicopter Society,* vol. 41, no. 4, pp 322-330, 1996.